Calibrating a large-scale groundwater model using spaceborne remote sensing products: a test-case for the Rhine-Meuse basin

EDWIN H. SUTANUDJAJA[1], LUDOVICUS P. H. VAN BEEK[1],
STEVEN M. DE JONG[1], FRANS C. VAN GEER[1,3] & MARC F. P. BIERKENS[1,2]

1 Department of Physical Geography, Faculty of Geosciences, Utrecht University, Utrecht, The Netherlands
e.sutanudjaja@geo.uu.nl
2 Unit Soil and Groundwater Systems, Deltares, Utrecht, The Netherlands
3 Netherlands Organization for Applied Scientific Research TNO, Utrecht, The Netherlands

Abstract The European Remote Sensing Soil Water Index (ERS SWI) fields, providing spatio-temporal soil moisture expressions, should be able to infer groundwater dynamics. In this study, we explore the possibility of using them to calibrate a coupled groundwater–land surface model. We apply a brute force calibration procedure by running several scenarios with varying parameter values of aquifer and upper soil properties. Results indicate that ERS SWI time series can be used in the calibration of such groundwater models by indirectly tuning groundwater recharge through changing the upper soil saturated hydraulic conductivities. It is shown that the scenarios showing good soil moisture dynamic performances also show good performances of their resulting groundwater head time series. However, the discharge performance is sensitive to the aquifer transmissivity. Discharge observations are thus also required for a more accurate model calibration.
Key words ERS Soil Water Index; soil moisture; remote sensing; groundwater head; discharge

INTRODUCTION

The current generation of large-scale hydrological models generally ignore a groundwater model component simulating groundwater lateral flows. Large-scale groundwater models are rare due to a lack of groundwater head data required for their calibration. Related to their coverage, such point scale groundwater head data are often so sparsely distributed that they must be interpolated. Consequently, large-scale groundwater modelling assessments are often complex and not accurate.

During the last decades, spaceborne remote sensing is increasingly being used for mapping and monitoring hydrological states and fluxes, such as precipitation, soil moisture, land surface temperature, snow cover, and evaporation and transpiration. The advantage of spaceborne remote sensing products is their global coverage. However, their benefits for groundwater hydrology must still be proven (Becker, 2006). Up to now, only the NASA GRACE (Tapley *et al.*, 2004) satellite has been acknowledged as a groundwater assessment tool, specifically for detecting groundwater storage dynamics (e.g. Rodell *et al.*, 2009). However, a major drawback of GRACE is its coarse resolution of 400 km, severely limiting its application. Groundwater hydrology is still exempt from spaceborne remote sensing applications (besides GRACE) because of an obvious reason: most current sensors are unable to penetrate sufficiently deep into the Earth to sense groundwater dynamics. Yet, Jackson (2002) reviewed the possibility of using a microwave sensor to estimate groundwater recharge due to its capacity to provide spatio-temporal surface soil moisture maps. Also, Becker (2006) argued that groundwater behaviours may be inferred from remotely sensed surface expressions, such as elevation, surface temperature and soil moisture. The latter is the focus of this study, in which the possibility of using a soil moisture product to calibrate a groundwater model is explored.

More specifically, the objective is to investigate whether a soil moisture product called the European Remote Sensing Soil Water Index (ERS SWI), introduced by Wagner *et al.* (1999), can be used to constrain a groundwater model. As the study area, we used the combined Rhine-Meuse basin (Fig. 1) that has a good coverage of ERS SWI and ample groundwater head observations that can be used to validate the model results. As the model, we adopted PCR-GLOBWB-MOD (Sutanudjaja *et al.*, 2011), which uses as input only global datasets so that the modelling procedure is portable to other areas in the world. In this study, which is our first attempt to calibrate the model, we implemented a brute force calibration by running several scenarios with varying parameter values. From them, we identified the parameter set that gives the best performance.
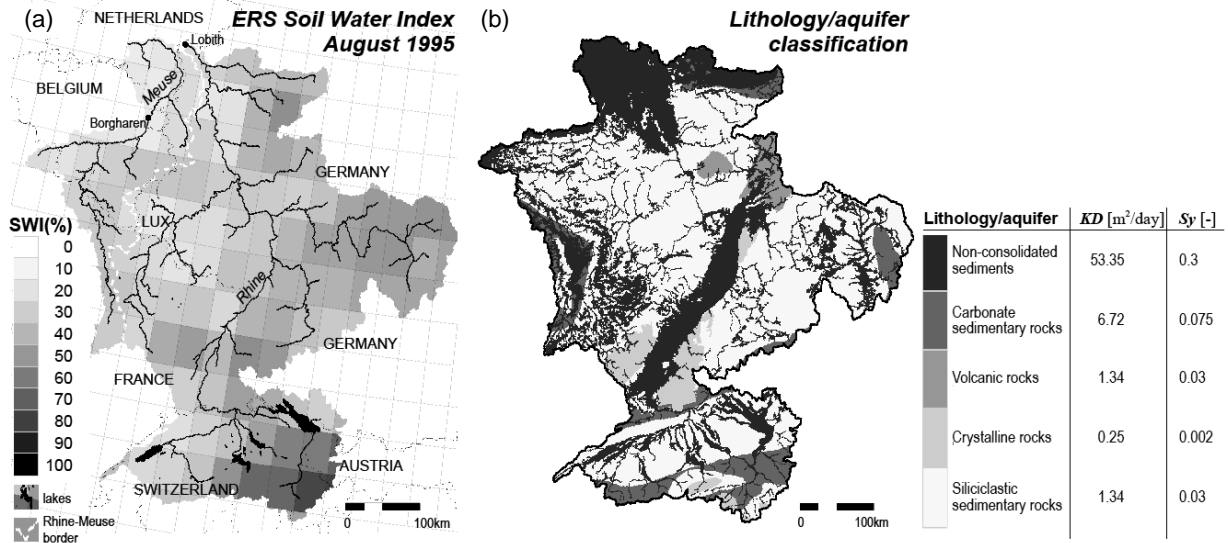
Fig. 1 The Rhine-Meuse basin used as the study area: (a) A snapshot of ERS SWI (Wagner *et al.*, 1999) in August 1995; (b) the aquifer classification (Dürr *et al.*, 2005; Sutanudjaja *et al.*, 2011) and parameters used in the reference scenario: *KD*: transmissivities, based on the global permeability values of Gleeson *et al.* (2011) and assuming the aquifer thickness equals to 50 m; *Sy*: specific yields, based on Freeze & Cherry (1979).

MODEL STRUCTURE

The PCR-GLOBWB-MOD

A detailed description of PCR-GLOBWB-MOD can be found in Sutanudjaja *et al.* (2011). We briefly describe its main features and report the modifications introduced in this present paper. Briefly stated, PCR-GLOBWB-MOD, which has the spatial resolution of 30 arc-second (about 1 km at the equator), is the land surface model PCR-GLOBWB (Van Beek & Bierkens, 2009) coupled to a MODFLOW (McDonald & Harbaugh, 1988) groundwater model. The land surface model conceptualizes the hydrological processes above and in two unsaturated zone soil layers (in which their storages are symbolized as S_1 and S_2 [L]), while the groundwater model contains a store (S_3 [L]) conceptualizing deeper saturated flows.

The land surface model of PCR-GLOBWB-MOD

In the stores S_1 and S_2, representing the top 30 cm (thickness $Z_1 \leq 30$ cm) and the following 70 cm ($Z_2 \leq 70$ cm) of soil, PCR-GLOBWB-MOD includes water balance calculations on a daily basis, a snow module based on HBV model (Bergström, 1995), an improved sub-grid saturation variability Arno scheme (Hageman & Gates, 2003) and an interflow module based on Sloan & Moore (1984). There are water exchanges between the first and second stores, Q_{12} [LT^{-1}], and between the second and groundwater stores, Q_{23} [LT^{-1}]. Q_{12} and Q_{23} consist of downward percolation fluxes, $Q_{1\rightarrow2}$ and $Q_{2\rightarrow3}$ [LT^{-1}], and capillary rise fluxes, $Q_{2\rightarrow1}$ and $Q_{3\rightarrow2}$ [LT^{-1}], that are driven by degrees of saturation of both stores, s [-], calculated either as $s = S/SC$ (where SC [L] indicates water storage capacities), or $s = \theta/\theta_{sat}$, (where the subscript "sat" indicates saturation and θ [-] is effective moisture content defined as $\theta = S/Z$ and $\theta_{sat} = SC/Z$). If there is enough water, percolation rate equals unsaturated conductivity, $K(s)$ [LT^{-1}]. If $s_1 < s_2$, capillary rise occurs with the amount of $Q_{2\rightarrow1} = K_2(s_2) \times (1-s_1)$. $K(s)$ is based on Campbell (1974): $K(s) = K_{sat} \times s^{2\beta+3}$, where β [-] is a parameter in the soil matric suction ψ [L] function of Clapp & Hornberger (1978): $\psi(s) = \psi_{sat} \times s^{-\beta}$.

In the previous PCR-GLOBWB-MOD (Sutanudjaja *et al.*, 2011), the capillary rise from the groundwater store is neglected ($Q_{3\rightarrow2} = 0$). In this present study, we activated it ($Q_{3\rightarrow2} \geq 0$). We adopted the Gardner-Eagleson approach (Gardner, 1958; Eagleson, 1978; Soylu *et al.*, 2011) to

estimate the capillary rise as a function of water table position. Given the assumptions of a steady state condition and that the suction head at the surface is (negatively) large (i.e. dry soil surface), the maximum capillary rise flux rate, v [LT^{-1}], is given as:

$$v = K_{\text{sat},2}\left[1+\frac{3}{(2+6/\beta_2)}\right]\left(\frac{|\psi_{\text{sat},2}|}{Z_{\text{gw}}}\right)^{2+3/\beta_2} \tag{1}$$

where Z_{gw} [L] is the difference of surface level (from the digital elevation model) and groundwater head h [L] (from the groundwater model). Equation (1) is used to estimate the maximum $Q_{3\rightarrow2}$ and limited by $K_{\text{sat},2}$, which is also used while the groundwater is at or above the surface ($Z_{\text{gw}} \leq 0$). Also, we limit that any capillary rise fluxes, including $Q_{3\rightarrow2}$ and $Q_{2\rightarrow1}$, do not result in the upper storage exceeding its equilibrium soil storage, W_{equ} [LT^{-1}]. The form of this equilibrium profile is given as (Clapp & Hornberger, 1978; Koster *et al.*, 2000):

$$s_{\text{equ}}(z)=\left(\frac{\psi_{\text{sat}}-z}{\psi_{\text{sat}}}\right)^{-1/\beta} \tag{2}$$

where s_{equ} [-] is the degree of saturation at a height z above the water table. The equilibrium soil storage W_{equ} is determined by integrating $s_{\text{equ}}(z)$ from the water table to the surface level.

Local runoff and channel discharge

The local runoff Q_{loc} [LT^{-1}] (from each 30 arc-second cell) consists of three components: direct runoff Q_{dr} [LT^{-1}] and sub-surface flow or interflow Q_{sf} [LT^{-1}] (from the land surface model part); and baseflow Q_{bf} [LT^{-1}] (from the groundwater model part, see the next sub-section). Given the area of each cell, A [L^2], we can express the local runoff in a water volume per unit Q_{tot} [L^{3}T^{-1}]:

$$Q_{\text{tot}} = A_{\text{cell}} \times \left[Q_{\text{dr}} + Q_{\text{sf}} + Q_{\text{bf}}\right]. \tag{3}$$

To obtain the channel discharge, Q_{chn} [L^{3}T^{-1}], we first accumulated Q_{tot} along the drainage network. Then, to take account of travel time through channels, the unit hydrograph method of the Soil Conservation Service (SCS, 1972; Sólyom & Tucker, 2004) was used to route discharge:

$$Q_{\text{chn,rt}}(t)=\sum_{n=0}^{N} f_n \times Q_{\text{chn}}(t-n) \tag{4}$$

where the subscript *rt* indicates the discharge after routing procedure implemented, t and $(t-n)$ are the current and previous daily time steps (until N days), and f [-] are the weights ($\Sigma f_n = 1$) given by considering the time of concentration at the most distant point of the basin to reach the cell.

Groundwater model

A single layer MODFLOW (McDonald & Harbaugh, 1988) groundwater model is coupled to the land surface model of PCR-GLOBWB-MOD. The MODFLOW model was forced by the output from the land surface model, specifically the net daily recharge $Q_{23} = Q_{2\rightarrow3} - Q_{3\rightarrow2}$ and the routed channel discharge $Q_{\text{chn,rt}}$ [LT^{-3}] that is beforehand translated to surface water levels HRIV [L] (see Sutanudjaja *et al.*, 2011). The "recharge" (RCH) package was used to introduce Q_{23}, while the "river" (RIV) and "drain" (DRN) packages were used to introduce HRIV as the boundary conditions of the MODFLOW model. The implementation of RIV and DRN packages gives the possibilities to quantify flows between streams and aquifers, symbolized as $-(\text{qRIV+qDRN})$ [LT^{-1}] (the negative sign "$-$" is used as MODFLOW assumes a positive sign for flows entering the aquifer). The amount of $-(\text{qRIV+qDRN})$, which depends on the difference between h and HRIV, is the main component of the baseflow Q_{bf}, especially for channels in flat sedimentary pockets where groundwater flows are slow. However, the magnitude of $-(\text{qRIV+qDRN})$ is too small to satisfy the baseflow originated from mountainous areas, where main flow sources often consist of many springs tapping groundwater located higher up in valleys (and feeding the head-water of

tributaries to main rivers). To include this fast component, we assumed that the groundwater above the flood plain is drained based on the linear reservoir concept. Hence, the total Q_{bf} is:

$$Q_{bf} = -(qRIV + qDRN) + (J \times S_{3,fpl})$$ (5)

where J [T^{-1}] is a reservoir coefficient parameterized based on Kraaijenhof van de Leur (1958) and $S_{3,fpl}$ [L] is the groundwater storage above the flood plain and calculated as:

$$S_{3,fpl} = \max(0, h - DEM_{fpl} + BUFF) \times Sy_{fpl}$$ (6)

where DEM_{fpl} [L] and BUFF [L] are the assumed flood plain elevation and storage buffer below the flood plain that can still contribute to baseflow, while Sy_{fpl} [-] is the assumed specific yield. As a consequence of incorporating this fast-response flow component – represented by the second term of equation (5) – the water balance of the model must be closed by subtracting this component from the input of the MODFLOW recharge package, RCH_{inp} [LT^{-3}]:

$$RCH_{inp} = (Q_{23} - J \times S_{3,fpl}) \times A_{cell}$$ (7)

Note all states and fluxes of this version of PCR-GLOWB-MOD are on a daily basis. We used an explicit scheme in equations (1)–(7), for which previous day values of h and $-(qRIV+qDRN)$ were used.

MODEL CALIBRATION/EVALUATION

ERS Soil Water Index, discharge and head data

Wagner *et al.* (1999) derived ERS SWI time series from the ERS Surface Soil Moisture (SSM) time series, which are retrieved 3–4 times per week. By employing an exponential low-pass filter to SSM time series, SWI time series were derived and provided in relative units (0–100%), representing the first metre soil moisture contents. SWI time series are available at 25–50 km and 10 day resolutions. However, we resampled them to 30 arc-minute (50 km at the equator) and 16 day resolutions to reduce the number of missing values that usually occur during the winter.

In this research, we compared the time series of the modelled saturation degree of the (entire) upper soil storage to the time series of ERS SWI. The saturation degree from the model, presented in the relative unit (0–100%), is simply calculated as s_{12} [-] = [S_1+S_2]/[SC_1+SC_2]. Comparisons are performed at the same spatial (30 arc-minutes) and temporal resolution (16 days). As a measure of likeliness, we considered the cross-correlation coefficient – symbolized as ρ_{SM} – between SWI and s_{12} time series. At this stage, we did not investigate the bias between them due to the discrepancy in the reference values. While the modelled s_{12} values range from zero (0%) to full saturation (100%), SWI values are assumed to be between wilting level (0%) and field capacity (100%), according to their product documentation (http://www.ipf.tuwien.ac.at/radar/index.php?go=ascat).

Besides evaluating the soil moisture, we also compared the calculated discharge $Q_{chn,rt}$ time series to the observation at two downstream locations: Lobith (Rhine) and Borgharen (Meuse). In both points, we determined the Nash & Sutcliffe (1970) efficiency coefficients in two ways: (1) using real discharge values (NS); and (2) using their logarithmic values (NS_LOG). While the first is to evaluate discharge peaks and high-flow events, we used the latter as a performance indicator of baseflow components and low flows. For verification, the modelled and observed groundwater head time series were also compared in >5000 stations. In each station, we calculated the correlation coefficient between modelled and observed head time series – symbolized as ρ_{HEAD}.

Model parameters and calibration strategies

The model was simulated for the period 1985–1999. We implemented a brute force calibration that may be considered a step-wise calibration procedure consisting of the two following steps.

As the first step, we ran 16 scenarios (see Table 1) with varying aquifer transmissivities *KD* [L^{2}T^{-1}] and exponents *b* [-] of the Arno scheme. The former is one of the MODFLOW parameters,

while the latter, which controls the partitioning of rainfall into direct runoff and infiltration to the soil, is defined in the land surface model. From the parameter b, it is expected that, for a given soil wetness, more direct runoff (and less infiltration) is produced if higher b values are introduced. Table 1 lists the (uniform) pre-factors of all scenarios, arbitrarily chosen and used to multiply the parameters of the reference scenario. For the parameters of the reference scenario (A), we adopted the values used in the previous PCR-GLOBWB-MOD (Sutanudjaja *et al.*, 2011), except for aquifer transmissivities, KD, and specific yields, Sy [-]. For KD values, we referred to Gleeson *et al.* (2011) who attributed the global lithological map of Dürr *et al.* (2005) with the geometric mean permeability of each lithology class in the map. For this study, the map used and its attribute values are given in Fig. 1(b). Note that, compared with the original map of Dürr *et al.* (2005), we simplified the number of classes into five and performed a series of corrections to include small aquifer structures and to correct the position of large aquifer bodies (see Sutanudjaja *et al.*, 2011). For Sy, the values were based on Freeze & Cherry (1979).

For the second calibration step, we identified one best scenario (based on ρ_{SM}, NS and NS_LOG) from the 16 scenarios defined in the first step (Table 1) and kept its KD and b values. Next, we performed 35 scenarios (Table 2) with varying values of Sy, K_{sat} and Z.

RESULTS

Table 1 lists the performance indicators (ρ_{SM}, NS and NS_LOG) during the first calibration set-up. The performance values are given in the (entire) basin scale-average values calculated by using the cells' areas as weight factors. In Table 1 we observed varying discharge performances measured by NS and NS_LOG. In terms of ρ_{SM}, all scenarios unfortunately show similar performance. Consequently, it is difficult to determine the optimal values of KD and b. It indicates that we should not only rely on ERS SWI time series while calibrating such a model. Other state variables and observation data (such as discharge) are definitely needed in order to calibrate models.

Table 1 Scenarios in the first step of calibration.

Code	KD	b	ρ_{SM}	NS		NS_LOG	
				Rhine	Meuse	Rhine	Meuse
A	1	1	0.59	0.44	0.54	−0.10	−5.57
B	1	0.01	0.58	0.52	0.52	−0.05	−5.59
C	1	0.1	0.58	0.51	0.52	−0.06	−5.60
D	1	1.5	0.59	0.39	0.54	−0.11	−5.51
E	0.1	1	0.59	0.43	0.47	0.45	−1.17
F	0.1	0.01	0.58	0.48	0.43	0.52	−1.03
G	0.1	0.1	0.58	0.48	0.43	0.51	−1.05
H	0.1	1.5	0.59	0.40	0.48	0.42	−1.22
I	0.5	1	0.59	0.48	0.55	0.18	−3.68
J	0.5	0.01	0.58	0.56	0.52	0.26	−3.58
K	0.5	0.1	0.58	0.55	0.52	0.25	−3.60
L	0.5	1.5	0.59	0.44	0.55	0.15	−3.69
M	10	1	0.59	0.28	0.39	−0.85	−10.45
N	10	0.01	0.58	0.34	0.36	−1.15	−11.13
O	10	0.1	0.58	0.24	0.36	−1.12	−11.08
P	10	1.5	0.59	0.24	0.40	−0.74	−10.07

* Tables 1 and 2 list the uniform pre-factors (KD, b, Sy, K_{sat}, Z) used to multiply the parameters of the reference scenario A and the model performance indicators (ρ_{SM}, NS, NS_LOG).
KD, transmissivities; b, Arno Scheme exponent; Sy, specific yield; K_{sat}, upper soil saturated conductivities; Z, upper soil depths; ρ_{SM}, correlation coefficients between calculated soil moisture and ERS SWI time series; NS and NS_LOG, Nash & Sutcliffe (1970) efficiency coefficients calculated using the absolute and logarithmic values of discharges.

Table 2 Scenarios in the second step of calibration.

Code	Sy	K_{sat}	Z	ρ_{SM}	NS		NS_LOG	
					Rhine	Meuse	Rhine	Meuse
F-101	0.75	0.01	0.75	0.48	−3.87	−2.00	0.11	−0.17
F-102	0.75	0.01	1	0.47	−3.81	−1.96	0.10	−0.17
F-103	0.75	0.01	1.25	0.45	−3.78	−1.95	0.10	−0.17
F-111	0.75	0.1	0.75	0.60	0.08	0.17	0.50	−0.15
F-112	0.75	0.1	1	0.58	0.22	0.33	0.49	−0.22
F-113	0.75	0.1	1.25	0.57	0.26	0.41	0.46	−0.37
F-121	0.75	1	0.75	0.56	0.35	0.38	0.52	−0.81
F-122	0.75	1	1	0.58	0.46	0.43	0.53	−0.86
F-123	0.75	1	1.25	0.60	0.50	0.45	0.52	−0.94
F-131	0.75	10	0.75	0.42	−0.62	−0.24	0.35	−1.63
F-132	0.75	10	1	0.48	−0.17	0.07	0.35	−1.84
F-133	0.75	10	1.25	0.50	0.05	0.17	0.34	−1.99
F-201	1	0.01	0.75	0.48	−3.89	−2.01	0.09	−0.26
F-202	1	0.01	1	0.47	−3.83	−1.98	0.08	−0.26
F-203	1	0.01	1.25	0.45	−3.79	−1.96	0.08	−0.26
F-211	1	0.1	0.75	0.60	0.09	0.18	0.48	−0.28
F-212	1	0.1	1	0.58	0.22	0.33	0.47	−0.35
F-213	1	0.1	1.25	0.57	0.25	0.40	0.44	−0.51
F-221	1	1	0.75	0.56	0.40	0.40	0.51	−0.98
F	1	1	1	0.58	0.48	0.43	0.52	−1.03
F-223	1	1	1.25	0.60	0.51	0.44	0.51	−1.12
F-231	1	10	0.75	0.42	−0.41	−0.10	−0.41	−1.84
F-232	1	10	1	0.47	−0.03	0.13	−0.03	−2.03
F-233	1	10	1.25	0.50	0.14	0.20	0.14	−0.17
F-301	1.25	0.01	0.75	0.48	−3.91	−2.03	−3.91	−0.32
F-302	1.25	0.01	1	0.47	−3.85	−1.99	−3.85	−0.33
F-303	1.25	0.01	1.25	0.45	−3.90	−2.18	−3.90	−0.36
F-311	1.25	0.1	0.75	0.60	0.09	0.19	0.09	−0.39
F-312	1.25	0.1	1	0.58	0.22	0.33	0.22	−0.48
F-313	1.25	0.1	1.25	0.57	0.24	0.40	0.24	−0.65
F-321	1.25	1	0.75	0.56	0.43	0.42	0.43	−1.15
F-322	1.25	1	1	0.58	0.50	0.44	0.50	−1.20
F-323	1.25	1	1.25	0.60	0.51	0.44	0.51	−1.29
F-331	1.25	10	0.75	0.42	−0.31	−0.08	−0.31	−2.03
F-332	1.25	10	1	0.47	0.57	0.17	0.57	−2.21
F-333	1.25	10	1.25	0.50	0.20	0.23	0.20	−2.35

* See the footnote below Table 1.
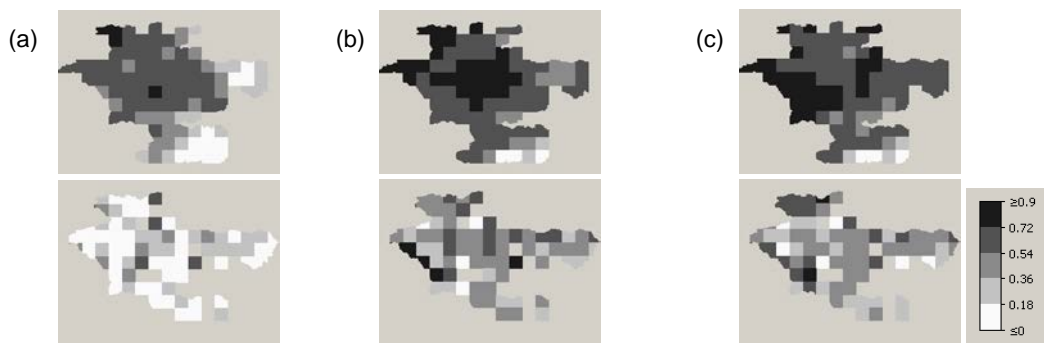
Fig. 2 Cross correlation fields between the calculated soil moisture and ERS SWI time series (ρ_{SM}) on the upper row; and between the calculated and measured groundwater head time series (ρ_{HEAD}) on the bottom row: (a) from the scenario F-202 (ρ_{SM} and ρ_{HEAD} in the basin average values equal to 0.47 and 0.16); (b) from the scenario F-212 (ρ_{SM} and ρ_{HEAD} in the basin average values equal to 0.58 and 0.44); and (c) from the scenario F (ρ_{SM} and ρ_{HEAD} in the basin average values equal to 0.58 and 0.40).

From Table 1, in terms of discharge performance measured by NS, most of the scenarios, except the ones with high transmissivities ($KD = 10KD_{ref}$, with the subscript "ref" indicating the reference scenario), show good performances, both in Rhine and Meuse ($NS_{Rhine} \geq 0.39$ and $NS_{Meuse} \geq 0.43$). However, in terms of NS_LOG, only scenarios with low transmissivities ($KD = 0.1KD_{ref}$) show reasonable discharge performances ($NS\_LOG_{Rhine} \geq 0.43$ and $NS\_LOG_{Meuse} \geq -1.22$). Hence, for the second calibration step, we used the scenario that has low transmissivities ($KD = 0.1KD_{ref}$). Unfortunately, determining the optimal b is difficult. From Table 1, given the same KD, scenarios with varying values of b provide similar performances of NS and NS_LOG. However, because we wanted to explore the influence of some other parameters (i.e. Sy, K_{sat} and Z), but limited the number of runs for computational reasons, we arbitrarily fixed b at 0.01 (following the scenario F).

For the second calibration step – summarized in Table 2 – in which we varied K_{sat}, Z and Sy, we identified that K_{sat} is the most sensitive parameter to the model performance indicators, while our variations of Z and Sy hardly influence them. Our variation of K_{sat} in Table 2 altered not only the discharge indicators NS and NS_LOG, but also the soil moisture performance indicator ρ_{SM}. It indicates the possibility to calibrate this parameter by evaluating the model results to SWI time series. In terms of ρ_{SM}, the scenarios with $K_{sat} = 0.1K_{sat,ref}$ and $K_{sat} = K_{sat,ref}$ are the best ones.

Figure 2 shows the fields of ρ_{SM} and ρ_{HEAD}, from three scenarios: F-202, F-212 and F. It shows that the scenarios that show good soil moisture performances also show good performance of their resulting groundwater heads. This shows the possibility of using ERS SWI to calibrate the model, but not directly through optimization of aquifer parameters (e.g. KD), but by tuning groundwater recharge through changing the upper soil saturated conductivities (K_{sat}).

CONCLUSIONS

Despite the limitations of this study, we have shown the possibility to determine a parameter value (i.e. K_{sat}) of a coupled groundwater–land surface model by comparing modelled soil moisture to ERS SWI time series. However, we also acknowledged that we were not able to fulfil the initial objective of our study, which is to calibrate the model by using only ERS SWI time series. Other datasets, such as discharge measurements (and possibly GRACE observations) should be included to calibrate the aquifer parameter (i.e. KD). These issues are subject to further study.

Photogrammetry and Remote Sensing, Vienna University of Technology, Austria (IPF TU Wien, http://www.ipf.tuwien.ac.at/radar).

REFERENCES

Bergström, S. (1995) The HBV model. In: *Computer Models of Watershed Hydrology* (edited by V. Singh). Water Resources Publications, Highlands Ranch, Colorado, USA.

Becker, M. W. (2006) Potential for satellite remote sensing of groundwater. *Ground Water* 44(2), 306–318, doi: 10.1111/j.1745-6584.2005.00123.x.

Campbell, G. (1974) A simple method for determining unsaturated conductivity from moisture retention data. *Soil Sci.* 117, 311–314.

Clapp, R. B. & Hornberger, G. M. (1978) Empirical equations for some soil hydraulic properties. *Water Resour. Res.* 14, 601–604.

Dürr, H. H., Meybeck, M. & Dürr, S. H. (2005) Lithologic composition of the Earth's continental surfaces derived from a new digital map emphasizing riverine material transfer. *Global Biogeochem. Cycles* 19, GB4S10, doi:10.1029/2005GB002515.

Gardner, W. R. (1958) Some steady state solutions of the unsaturated moisture flow equation with application to evaporation from a water table. *Soil Sci.* 85, 244–249.

Eagleson, P. (1978) Climate, soil, and vegetation: 3. A simplified model of soil moisture movement in the liquid phase. *Water Resour. Res.* 14, 722–730.

Freeze, A. R. & Cherry, A. J. (1979) *Groundwater*. Prentice Hall.

Gleeson, T., Smith, L., Moosdorf, N., Hartmann, J., Dürr, H. H., Manning, A. H., van Beek, L. P. H., & Jellinek, A. M. (2011) Mapping permeability over the surface of the Earth. *Geophys. Res. Lett.* 38, L02401, doi:10.1029/2010GL045565.

Hagemann, S. & Gates, L. D. (2003) Improving a subgrid runoff parameterization scheme for climate models by the use of high resolution data derived from satellite observations. *Clim. Dynam.* 21, 349–359.

Jackson, T. (2002) Remote sensing of soil moisture: implications for groundwater recharge. *Hydrogeology J.* 10, 40–51, doi:10.1007/s10040-001-0168-2.

Koster, R. D., Suarez, M. J., Ducharne, A., Stieglitz, M., & Kumar, P. (2000) A catchment-based approach to modeling land surface processes in a general circulation model 1. Model structure. *J. Geophys. Res.*, 105(D20), 24809–24822, doi:10.1029/2000JD900327.

Kraaijenhoff van de Leur, D. (1958) A study of non-steady groundwater flow with special reference to a reservoir coefficient, *De Ingénieur* 70, 87–94.

McDonald, M. & Harbaugh, A. (1988) A modular three-dimensional finite-difference ground-water flow model: Techniques of Water Resources Investigations of the United States Geological Survey, Book 6, http://pubs.water.usgs.gov/twri6a1.

Nash, J. E. & Sutcliffe, J. V. (1970) River flow forecasting through conceptual models part I – A discussion of principles. *J. Hydrol.* 10(3), 282–290, doi:10.1016/0022-1694(70)90255-6.

Rodell, M., Velicogna, I. & Famiglietti, J. S. (2009) Satellite-based estimates of groundwater depletion in India. *Nature* 460(7258), 999–1002, doi:10.1038/nature08238.

SCS, Soil Conservation Service (1972) *National Engineering Handbook*, Section 4. US Department of Agriculture.

Sloan, P. G. & Moore, I. D. (1984) Modeling subsurface stormflow on steeply sloping forested watersheds. *Water Resour. Res.* 20, 1815–1822.

Sólyom, P. B. & G. E. Tucker (2004) Effect of limited storm duration on landscape evolution, drainage basin geometry, and hydrograph shapes. *J. Geophys. Res.* 109, F03012, doi:10.1029/2003JF000032.

Soylu, M. E., Istanbulluoglu, E., Lenters, J. D. & Wang, T. (2011) Quantifying the impact of groundwater depth on evapotranspiration in a semi-arid grassland region. *Hydrol. Earth Syst. Sci.* 15, 787–806, doi:10.5194/hess-15-787-2011.

Sutanudjaja, E. H., van Beek, L. P. H., de Jong, S. M., van Geer, F. C. & Bierkens, M. F. P. (2011) Large-scale groundwater modeling using global datasets: a test case for the Rhine-Meuse basin. *Hydrol. Earth Syst. Sci.* 15, 2913–2935, doi:10.5194/hess-15-2913-2011.

Tapley, B. D., Bettadpur, S., Ries, J. C., Thompson, P. F. & Watkins, M. M. (2004) GRACE measurements of mass variability in the Earth system. *Science* 305(5683), 503–505.

Van Beek, L. P. H. & Bierkens, M. F. P. (2009) The Global Hydrological Model PCR-GLOBWB: Conceptualization, Parameterization and Verification, Report, Department of Physical Geography, Utrecht University, Utrecht, The Netherlands, http://vanbeek.geo.uu.nl/suppinfo/vanbeekbierkens2009.pdf, (last accessed 10 August 2011).

Wagner, W., Lemoine, G. & Rott, H. (1999) A method for estimating soil moisture from ERS Scatterometer and soil data. *Remote Sensing of Environ.* 70(2), 191–207.